Three-dimensional simulations of a planet embedded in a protoplanetary disk

Wilhelm Kley[1]

Max-Planck-Institut für Astronomie, Königstuhl 17, D-69121 Heidelberg, Germany

kley@mpia-hd.mpg.de

and

Gennaro D'Angelo and Thomas Henning

Astrophysikalisches Institut und Universitäts-Sternwarte, Friedrich-Schiller-Universität, Schillergäßchen 2-3, D-07745 Jena, Germany

gennaro@astro.uni-jena.de, henning@astro.uni-jena.de

ABSTRACT

The dynamical influence of Jupiter-sized planets still embedded in protostellar disks is studied by means of numerical simulations. The three-dimensional structure of the disk is fully taken into account. Assuming a disk mass of $3.5 \times 10^{-3} M_\odot$ within 2 and 13 AU, typical values for the vertical thickness $H/r = 0.05$ and viscosity of the disk $\alpha \approx 4 \times 10^{-3}$, we find for the mass accretion rate onto the planet a value of $6 \times 10^{-5} M_{Jup}/yr$ and for the the migration timescale a value of $10^5 yr$. These results are in excellent agreement with previously obtained results from two-dimensional calculations of infinitesimally thin disks. We argue that this agreement is to be expected if the vertical height of the disk is similar or smaller than the size of the Roche-lobe of the embedded planet.

Three-dimensional models having a lower planetary mass or different H/r values display small deviations from two-dimensional results.

Subject headings: accretion — hydrodynamics — planetary systems

1. Introduction

Since the discovery of the first extrasolar planet around a main-sequence star 5 five years ago by Mayor & Queloz (1995), the field of planet searching has grown dramatically. Today over 40

[1]New address: Institut für Astronomie und Astrophysik, Universität Tübingen, Auf der Morgenstelle 10, D-72076 Tübingen, Germany

extrasolar planets are known. For a summary, we refer to Marcy, Cochran & Mayor (2000). An always up-to-date status of extrasolar planets can be found at the *Extrasolar Planet Encyclopedia*, maintained by J. Schneider at http://www.obspm.fr/planets.

The main difference to our own Solar System, where planets have rather small masses and orbit the sun on nearly circular orbits at distances of several AU, has been the discovery of massive planets with minimum masses up to 10 Jupiter masses (M_{Jup}). Some of the newly discovered planets orbit their central stars very closely (within a tenth of an AU) on orbits with very small eccentricities. For larger semi-major axis the eccentricities tend to be larger with a maximum of 0.67. The only extrasolar planetary system around a main-sequence star known so far (υ And) consists of one planet at 0.059 AU on a nearly circular orbit and two planets, at 0.83 and 2.5 AU, having larger eccentricities (0.18 and 0.41) (Butler et al. 1999).

These rather unexpected findings have brought new momentum into the field of planet formation, and theorists have begun to explore the physical conditions under which planets are supposed to form. Stars are formed through the gravitational collapse of a molecular cloud core. Angular momentum conservation leads to the formation of a circumstellar disk around the protostar, where mass is slowly transported inwards and accreted by the star.

It is generally agreed that planets form within these disks, either by direct fragmentation through gravitational instability (Boss 1998), or through coagulation from solid material within the disk and subsequent growth through inelastic collisions and gas accretion from the disk (Beckwith, Henning & Nakagawa 2000). In this scenario all of the newly created planets orbit the star essentially on circular orbits as they originate from a Keplerian disk and, the more massive, gaseous planets tend to have distances of several AU from the star.

While this scenario explains well the observational data of the Solar System, it does not match so well the new results on the extrasolar planets. As the last phase of planet formation determines the final masses and orbital elements of the planets, it seems essential to concentrate in particular on this final evolutionary stage.

By now, several numerical computations of planets embedded in infinitesimally thin two-dimensional ($r - \varphi$) gaseous disks have been carried out. The basic features of the flow within the perturbed disk and the mass accretion rate onto the planet has been studied for planets on fixed circular orbits by Bryden et al. (1999), Kley (1999) and Lubow, Seibert & Artymowicz (1999). Additionally, the back reaction of the disk onto the planet's orbital elements has been analyzed by Nelson et al. (2000) and Nelson & Benz (1999), and the dynamical influence of a secondary planet was studied by Kley (2000). Hydrodynamic calculations of embedded low mass planets (type I migration) were performed in two and three dimensions by Miyoshi et al. (1999) using a local approximation.

While the dynamical properties of the disk may be described adequately by the two-dimensional (2D) assumption, it appears questionable if the dynamics of the flow in the vicinity of the planet and the mass accretion onto it can be described satisfactorily by this approach. To elucidate on

this issue we performed fully three-dimensional (3D) simulations of Jupiter-sized planets embedded in a disk, where we resolve the vertical structure of the disk. These results are compared with two-dimensional models. Crucial for the evolution of planet is the question of mass growth and migration, which may depend on planetary as well as disk properties. We calculate the mass accretion and migration rate of the embedded planet for different planet masses and varying disk thickness.

In Section 2, we explain our model by stating the physical assumptions and approximations. In Section 3, we first present a test calculation analyzing the ability of the code to describe 3D disks, and then present results for the complete case including the planet. Our conclusions are given in the last section 4.

2. The Model

In calculating the dynamical evolution of an accretion disk, it is usually assumed that the mean free path between individual particles is small compared to the overall extent of the disk. Thus, the evolution is described best by the hydrodynamic approximation including viscosity, i.e. the Navier-Stokes equations. Here, we consider a full three-dimensional model which includes the vertical extension of the disk.

The disk is non-self-gravitating and is orbiting a protostar having a mass of $1M_{\odot}$. The total mass of the disk within the simulated region, 2.08 to 13 AU, is $3.5 \times 10^{-3} M_{\odot}$. Embedded in this disk is a massive protoplanet of typically $1M_{Jup}$ but a smaller mass of $0.5M_{Jup}$ has been considered as well. The planet is assumed to be on a fixed circular orbit throughout the evolution.

2.1. Basic equations

Suited best for this problem are spherical polar coordinates (R, θ, φ) where R denotes the radial distance from the origin, θ the polar angle measured from the z-axis, and φ denotes the azimuthal coordinate starting from the x-axis.

In this coordinate system, the midplane of the disk coincides with the equator ($\theta = \pi/2$), and the origin of the coordinate system, $R = 0$, lies in the center of mass of the star and planet. Sometimes we will need the radial distance from the polar axis which we denote by a lower case r, which is the radial coordinate in cylindrical coordinates.

For a better resolution of the flow in the vicinity of the planet, we work in a rotating coordinate system which rotates with the orbital angular velocity Ω, which is identical to the orbital angular velocity of the planet

$$\Omega_P = \left[\frac{G\,(M+m)}{a^3} \right]^{1/2} \tag{1}$$

where M is the mass of the star, m the mass of the planet, and a is the semi-major axis of the planet. For the sake of comparison, we calculated additional models in the inertial frame.

The full hydrodynamic equations, including the viscous terms, spelled out in spherical polar coordinates can be found for example in Tassoul (1978). However, as we use here a more conservative variant of the momentum equations including a rotating frame of reference we quote them explicitely:

a) Radial Momentum

$$\frac{\partial \rho\, u_R}{\partial t} + \nabla \cdot (\rho\, u_R\, \mathbf{u}) = \rho \frac{u_\theta^2}{R} + \rho\, \sin^2\theta R(\omega+\Omega)^2 - \frac{\partial p}{\partial R} - \rho\, \frac{\partial \Phi}{\partial R} + f_{\rm R}; \tag{2}$$

where ρ denotes the density of the gas, $\mathbf{u} = (u_R, u_\theta, u_\varphi)$ is the velocity of the gas, ω is the azimuthal angular velocity as measured in the rotating frame, p is the gas pressure, and Φ denotes the gravitational potential due to the star and the planet.

b) Meridional Momentum

$$\frac{\partial (\rho\, R\, u_\theta)}{\partial t} + \nabla \cdot (\rho\, R\, u_\theta\, \mathbf{u}) = \rho R^2 \sin\,\theta \cos\,\theta (\omega+\Omega)^2 - \frac{\partial p}{\partial \theta} - \rho\, \frac{\partial \Phi}{\partial \theta} + f_\theta \tag{3}$$

c) Angular Momentum

$$\frac{\partial \rho\, h_t}{\partial t} + \nabla \cdot (\rho\, h_t\, \mathbf{u}) = -\frac{\partial p}{\partial \varphi} - \rho\, \frac{\partial \Phi}{\partial \varphi} + f_\varphi; \tag{4}$$

where we defined the *total* specific angular momentum

$$h_t = R^2\, \sin^2\theta\, (\omega+\Omega)\,; \tag{5}$$

i.e. the azimuthal velocity in the rotating frame is given by $u_\varphi = \omega\, R\, \sin\theta$.

The Coriolis force of the last equation for u_φ has been incorporated into the left hand side. Thus, it is written in such a way as to conserve total angular momentum best. This conservative treatment is necessary to obtain an accurate solution of the embedded planet problem (Kley 1998).

The function $\mathbf{f}$ includes the viscous forces which are stated explicitly for the three-dimensional case in spherical polar coordinates by Klahr, Henning & Kley (1999). For the description of the viscosity we assume a Reynolds stress-tensor approach with a constant kinematic viscosity coefficient ν having the value 10^{-5} in dimensionless units where $a = 1$ and $\Omega_P = 1$ (see Appendix), which translates into a Reynolds number of 10^5. For the given vertical thickness of the disk ($H/r = 0.05$) this value for ν is equivalent to $\alpha \approx 4 \times 10^{-3}$ at $R = a$.

For simplicity, to avoid any complications due to internal heating and radiative transport, we treat here only disks with a specified temperature distribution (see below).

2.2. Initial setup

The initial disk is assumed to be axisymmetric with respect to the polar axis, $\theta = 0$, of the coordinate system. The gas moves with Keplerian velocity around the central star and has no radial and vertical motion; that means at $t = 0$ the velocity is $\mathbf{u} = [0, 0, R(\Omega_K - \Omega)]$, where Ω_K is the Keplerian angular velocity of the gas, $\Omega_K = (GM/r^3)^{1/2}$, and we have included the correction caused by the rotating coordinate frame. For simplicity we neglect any vertical dependence of u_φ in the initial conditions because the vertical thickness H of protoplanetary disks at a given distance r from the center is typically very small compared to the radius.

Here we assume that the disk has a *constant* relative thickness $h = H/r$ at all radii. This is usually a good approximation for accretion disks since detailed vertical models give for regions which are not flared a very weak dependence of H/r with radius, typically $H/r \propto r^{0.1}$. Here we choose three different values ranging from $H/r = 0.05$ upto $H/r = 0.15$. A thin Keplerian disk is radially in equilibrium as gravitational and centrifugal forces approximately balance because pressure effects are small. The vertical structure can be obtained from the equation of hydrostatic equilibrium (in cylindrical coordinates). If one assumes that the disk is thin and is locally isothermal, $T = T(r)$, one finds easily that the local vertical density profile is given by a Gaussian (Frank, King & Raine 1992). Hence, neglecting again geometry effects, we use for the initial density

$$\rho(t = 0) = \frac{\rho_0}{(r/r_0)^{3/2}} \exp\left(-\frac{\vartheta}{h}\right)^2 \tag{6}$$

where $\vartheta = \pi/2 - \theta$ is the polar angle measured from the midplane of the disk. The constant ρ_0 which sets the total mass of the disk is arbitrary as long as no back-reaction of the disk onto the orbit of the planet or self gravity is taken into account. Here, we adjust ρ_0 such that the total mass of the disk within the computational domain (from 2.08 to 13.0 AU) is $M_d = 3.5 \times 10^{-3} M_\odot$. The radial dependence has been chosen such that the vertically averaged density $\Sigma(r) = \int_{-\infty}^{+\infty} \rho dz$, the surface density, falls off as $r^{-1/2}$. This allows a direct comparison of the new three-dimensional results with previous two-dimensional computations (Kley 1999). The constant r_0 is some reference radius. The temperature law follows from the constancy of h, and is given by $T(r) \propto r^{-1}$.

The planet with mass $1 M_{Jup} = 0.001 M_\odot$ is located at $R = 5.2$ AU and, since we are working in the corotating frame, at the fixed azimuthal angle $\varphi = \pi$. Some numerical issues such as grid size and dimensionless quantities are described in the appendix.

The standard model (Sect.3.2) refers to a modest resolution of ($128 \times 128 \times 20$) gridcells. However, to test the reliability of this apparently low resolution concerning the accretion and migration rate (torque) we also considered higher resolution models with with different physical parameters, as given in Table. 1 below. We note that, using the standard resolution, there are about 4.5 radial and only 1.7 azimuthal gridcells within the Roche-lobe of the planet. However, since mass is taken out continuously from the middle of the Roche-lobe we believe that this resolution may be sufficient to yield reliable results. This is tested by higher resolution cases, which give in fact essentially the same results for the mass accretion and the migration rate. The mass accretion onto

the planet is modeled by reducing the density in the inner half of the Roche-lobe by a given fraction per timestep (see Appendix).

3. Results

As this is the first application of the code to three-dimensional disks we present in the beginning results of a test calculation where we study the evolution of a section of a disk without a planet towards equilibrium. Then we describe our results obtained for the full embedded planet case.

3.1. A test case

We start with an initially constant density ρ = const configuration rotating with Keplerian speed around the star. The radial and vertical velocities have been set to zero initially. For the given temperature profile which is constant on θ = const.-surfaces we expect the vertical density profile to become Gaussian (see above) and for the surface density Σ the final radial distribution should follow $\Sigma(r) \propto r^{-1/2}$.

In Fig. 1 we display the radial dependence of the azimuthally averaged surface density at different times. We note that during the total time evolution during 500 orbits or 200000 timesteps the azimuthal asymmetry did not grow beyond 10^{-13}. At $t = 0$, the constant three dimensional density yields a profile $\Sigma_0(r) \propto r$. During the evolution towards equilibrium sound waves are generated which are slowly damped by the viscosity, and finally the density profile approaches the analytic solution.

The viscous damping is illustrated in Fig. 2 where the time evolution of the total kinetic energy of the radial and vertical velocity components is displayed. After a brief fast initial decline due to non-linear effects, the decay proceeds on the long viscous timescale. The evolution towards vertical equilibrium is displayed in Fig. 3 where we plot the vertical density distribution at $r = 1$ at different evolutionary times. As expected from hydrostatic equilibrium, the vertical structure settles for the constant temperature to a Gaussian distribution.

3.2. A $1M_{Jup}$ planet embedded in a disk with $H/r = 0.05$

Now we first consider our standard case of a $1M_{Jup}$ planet embedded in a disk with the constant vertical height $H/r = 0.05$, equivalent to a Mach number of 20 throughout the disk. As described above we start from an initially axisymmetric configuration with a gap imposed (see also Fig. 7 below). Gravitational interaction of the planet with the disk leads to the creation of tightly wound trailing spiral density waves.

In Fig. 4 the overall structure of the surface density Σ is displayed after 150 orbits of the planet. The spirals emanate from the vicinity of the planet and reach the outer boundary. Since the radial outer boundary is closed to mass flow, there the waves are reflected, which is more clearly seen in the right panel of Fig. 4. This reflection is somewhat larger for the computations performed here than that observed in previous calculations (Kley 1999, code RH2D) because the computational domain is smaller. The use if this smaller domain with the increased reflection properties does not change the accretion and migration properties of the planet significantly, as they are determined by the flow structure in the vicinity of the planet.

In the region outside of the planet two spirals are inter-twined and in the inner region three. This difference is caused by the location of the appropriate Lindblad resonances in comparison to the radial extent of the gap. Only resonances which are located further away from the planet than the gap size can be excited effectively.

In Fig. 5 the density slice $\rho(R, \theta, \pi)$ is shown at $t = 150$ orbits. In addition, the two-component velocity field (u_R, u_θ) is shown. Inside the gap, around $R = 1$, the flow field is definitely directed towards the midplane of the disk, onto the planet. Even from the furthermost grid cells, at $R \approx 1$, the velocity points to the position of the planet. This implies that all the fluid elements, along the vertical direction, are involved in the planet accretion process as it is assumed when adopting a 2D approximation. This can be attributed to two facts: 1) Because of the continuous mass extraction from within the Roche lobe, the vertical hydrostatic balabce is lost which allows material all heights to fall down onto the planet, and 2) The effective potential causes the gas flow to pass near the Lagrangian equilibrium points which are located in the equatorial plane, hence the gas flow will be directed towards the planet in its vicinity.

Clearly seen in Fig. 5 are also the locations of the spiral waves which show up as density enhancements reaching from the midplane of the disk all the way down to the surface. At all heights the arms are at the same radial position because in case of the isothermal assumption the wave propagation speed is the same at all heights. Caused by the closed inner boundary condition the density becomes very large near $R_{min} = 0.4$

At each side of the planet, a column of material is also visible, it extends from $\theta = 0$ to $\theta \simeq 0.05$. Though not very well resolved in the radial direction, this material might be contained within the Hill sphere of the planet which, in the present case, has a radius of $\simeq 0.069$ in dimensionless units. From the velocity field, it seems that the fluid elements belonging to these structures, move towards the planet according to bow-shape stream lines. In Fig. 6 we plot the density structure in the $\theta - \varphi$ plane at the planet's location $R = 1$ for the same model. Also here the loss of vertical hydrostatic equilibrium is reflected by the vertically downward motion of the gas.

The radial dependence of the surface density is shown in Fig. 7 together with other simulations using always identical *physical* parameters. The initial density profile is given by the dark dotted line. We use two different codes RH2D (labeled 2D: solid lines) and Nirvana (labeled N2D: dashed lines; N3D: dashed-dotted lines) where we use the latter one in a 2D setup and in the previously

described 3D setup. Each of the three models is run in the inertial and the corotating frame. The initial total matter content of the models has been adjusted to agree in all cases. Clearly the overall agreement of all models is very good, the shape of the gap is identical for all models. The only difference is that the models run with Nirvana show a larger variation at the outer radial boundary (at $R = 2.5$) which is an indication of a stronger wave reflection in the Nirvana code, possibly due to slightly different boundary conditions. The good agreement of the different models is corroborated in Fig. 8 where we plot the obtained total mass accretion rate $\dot{M}_p$ onto the planet for the different models. Only for the corotating 3D cases the obtained $\dot{M}_p$ appears to be slightly but not significantly higher. The accretion rate does not depend on the chosen resolution as is shown by the higher resolution model (384 azimuthal gridcells, otherwise identical to N3d rot.) which has been run only until $t \approx 100$ due to limited computational resources.

The gravitational force $\mathbf{F}$ of the disturbed non-axisymmetric density distribution of the disk creates a torque $\mathbf{T} = \mathbf{r} \times \mathbf{F}$ on the planet, which eventually alters its orbital elements. For the present work however, these changes have no dynamical influence, because we assume that the planet remains on a fixed circular orbit. The resulting radial distribution of the vertical $z-$component of the torque is shown, as a solid line, for the standard 3D-model (N3D rot.) in Fig. 9. It shows a strong variation (spikes) with radius that is caused by the spiral density structure. The Figure shows also the same quantity as obtained from the N2D rot. model. As one can see, the two curves have slightly different shapes only close to the planet (at $R \approx 0.9$ and $R \approx 1.1$), where the 3D result is less variable.

The total torque $T_\perp$ can be obtained by integrating $T_z(r)$ over all radii. An applied torque on the planet changes its angular momentum $L_p = m\, a^2\, \Omega_P$ and leads to a change in its semi-major axis

$$\dot{a} = \frac{2}{a\, M_{pl}\, \Omega_P}\, T_\perp. \tag{7}$$

As the direction of the motion is determined by the sign of the total torque, it is clear already from Fig. 9 that the planet will migrate inwards. The main contribution to this lowering of a comes from the density in the trailing spiral arm near the outer edge of the gap. The deep minimum at $r \approx 1.7$ refers to the $2:1$ outer Lindblad resonance. It has been demonstrated already (Lubow, Seibert & Artymowicz 1999; Nelson et al. 2000) that the material lying at radii larger than the planet's semi-major axis tend to move the planet inward while inner material has the opposite effect. As there is typically more mass (larger area) in the outer region the net effect will be an inward migration of the planet. For the timescale of this migration

$$\tau_{mig} = \frac{a}{|\dot{a}|}$$

we find for *all* the models $\tau_{mig} \approx 10^5 yr$ if we assume a total disk mass within $[r_{min}, r_{max}]$ of $3.5 \times 10^{-3} M_\odot$. This compares favourably with the analytic results of Goldreich & Tremaine (1980) based on a linear analysis which results for the same disk density also in a time scale of about 10^5yrs. The dynamical evolution of migrating planets has been studied in detail by Nelson et al. (2000).

3.3. Varying the disk height and the planetary mass

We have also run models with smaller planet masses and higher $H/\,r$ ratios. The parameters of some of such models are listed in table 1. For all of them the boundary conditions at inner radial border are such that they allow matter to outflow from the computational domain but not to inflow. For each set of physical parameters we have performed two- and three-dimensional calculations at much higher resolution than standard test case in the previous section. As can be seen from the table we have chosen the number of gridcell in the azimuthal $\varphi-$direction such as to make the gridcells approximately square shaped, which required $N_\varphi = 384$ gridcells. The number of gridcells in the vertical direction was higher for the model P3 ($N\theta = 30$) because of the larger H/r.

In case of the Models A and B the ratio of the Hill radius (R_H) to the local thickness of the disk is almost unity. One can see that, after 200 orbits, the 3D model accretion rate (Fig. 10, left panel) is 12% less than that of the corresponding 2D model. For Models C and D (Fig. 10, central panel) the ratio $R_H/\,h$ decreases to 0.7 and the two curves show a difference of 10%. In the right panel of the same Figure one can clearly see that, dispite the difference in azimuthal resolution, the 2D model (P2a and P2b) results differ very little, while the 3D one lies almost the 30% below. These comparisons show that whenever $R_H/\,h \leq 1$, the 2D approximation starts to break down and the 2D accretion rates lie consistently above the 3D values. The migration timescale for the smaller models (A, B) are about $10^5\,yrs$ while for models with higher disk thickness the results are very noisy but indicate somewhat longer timescales.

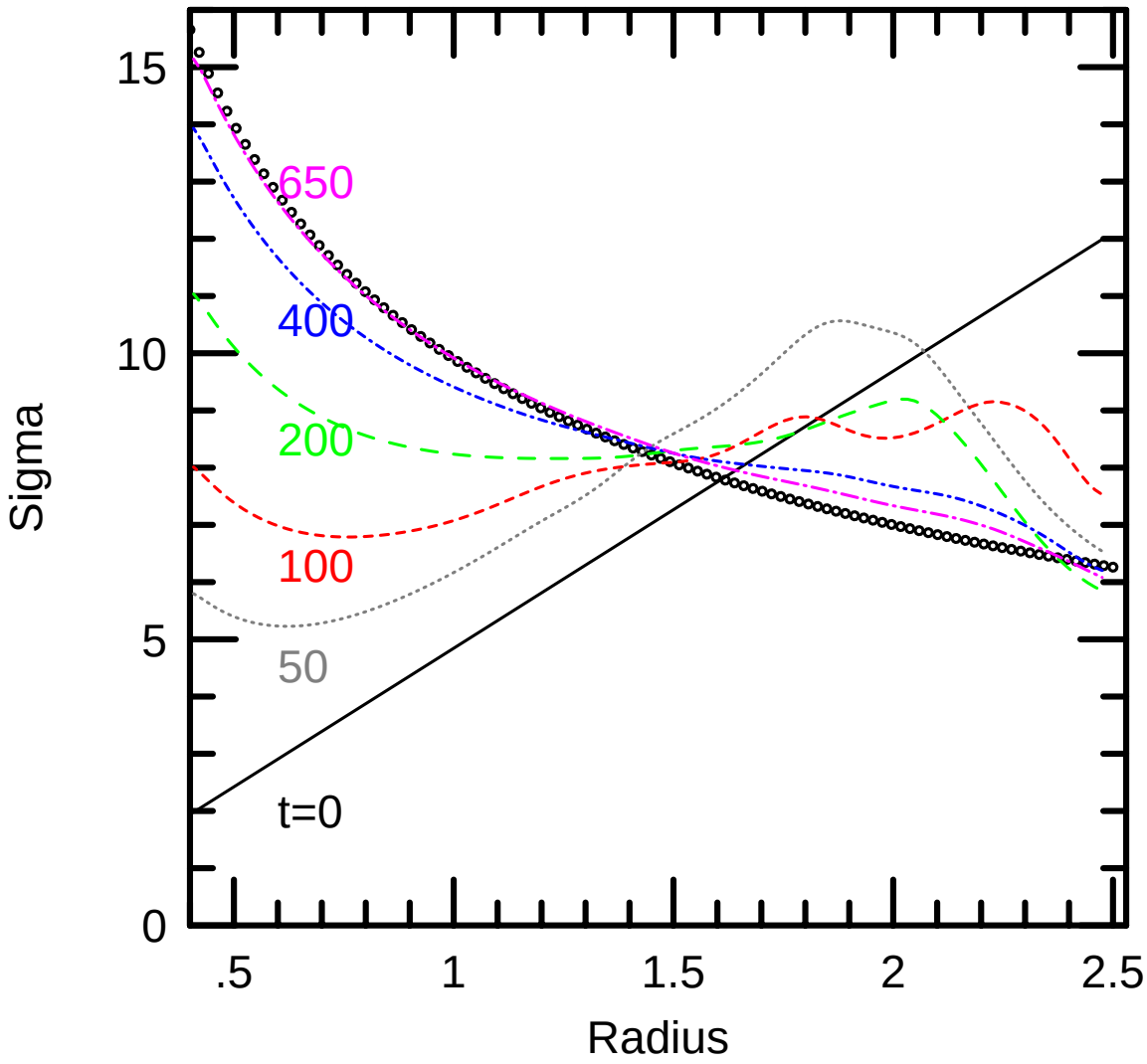

Fig. 1.— Vertically averaged density $\Sigma(r)$ at different times for the test model with no planet and an initially constant three-dimensional density. At late times $\Sigma(r)$ approaches the analytic profile (circles).

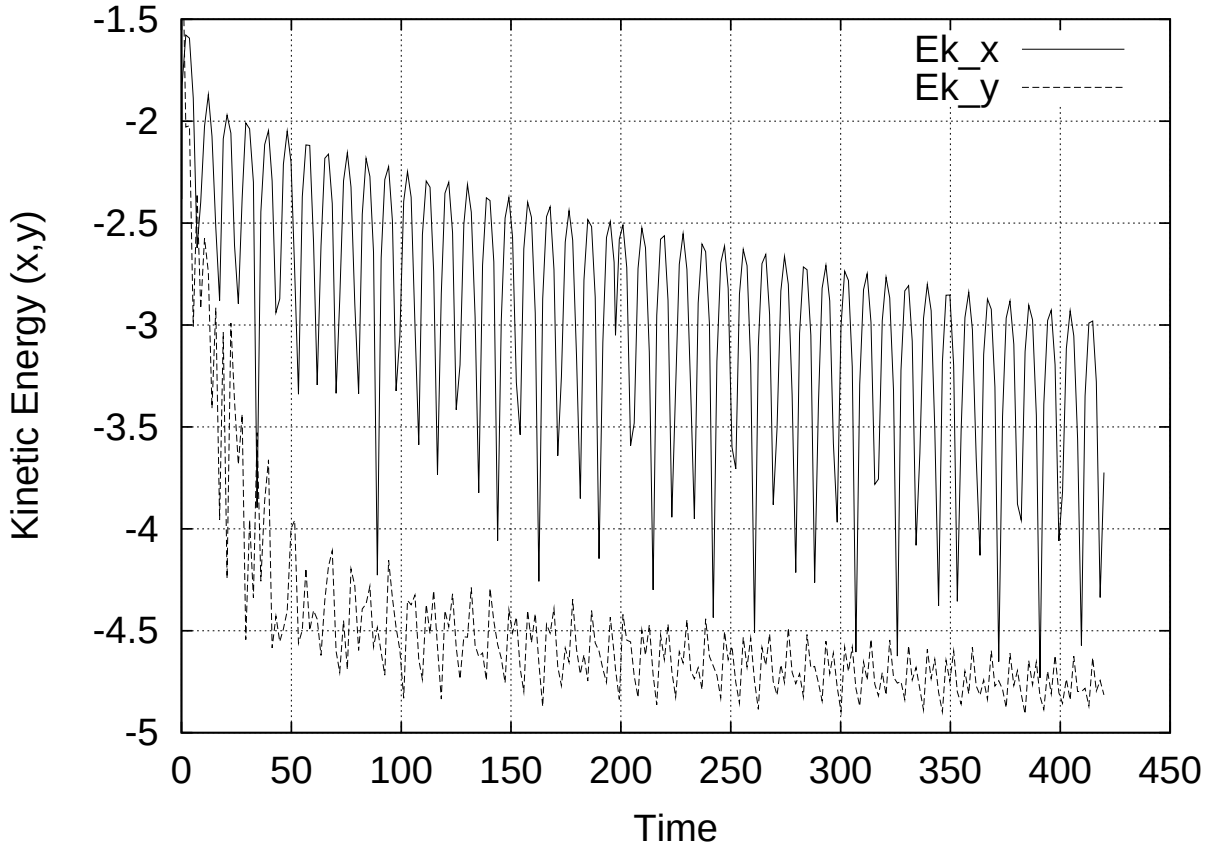

Fig. 2.— The time evolution of the total kinetic energies in the radial (x) and meridional (y) direction.

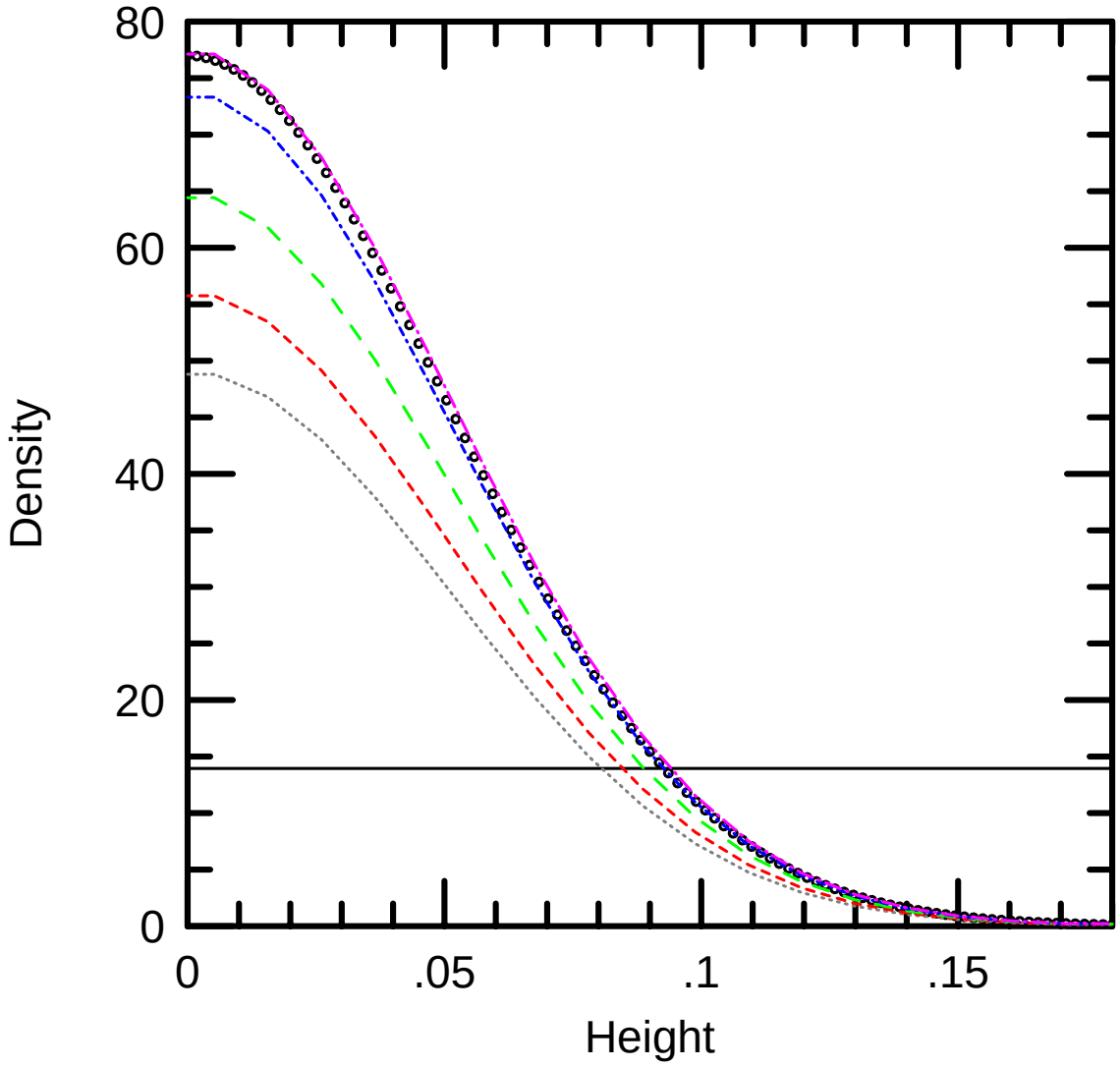

Fig. 3.— The vertical dependence of the density at $r = 1$ at various times. Starting from the initial constant density configuration, the final distribution becomes Gaussian (circles) as expected (circles). The evolutionary times are identical to Fig. 1

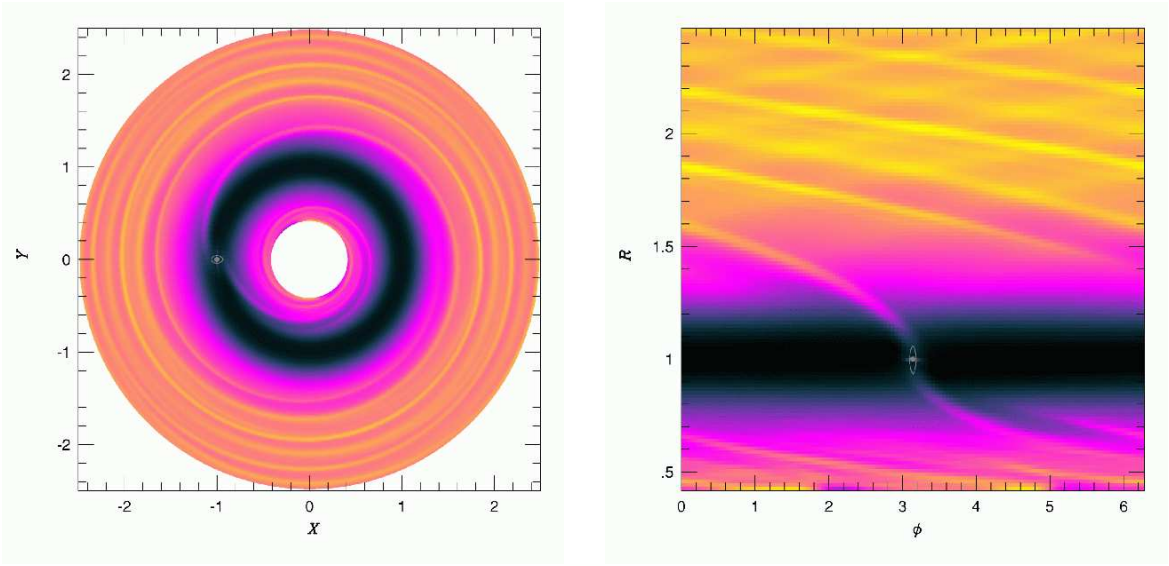

Fig. 4.— The surface density distribution at $t = 150$ orbits. Left in Cartesian $x - y$ coordinates, right in radial and azimuthal coordinates ($r - \varphi$ plane).

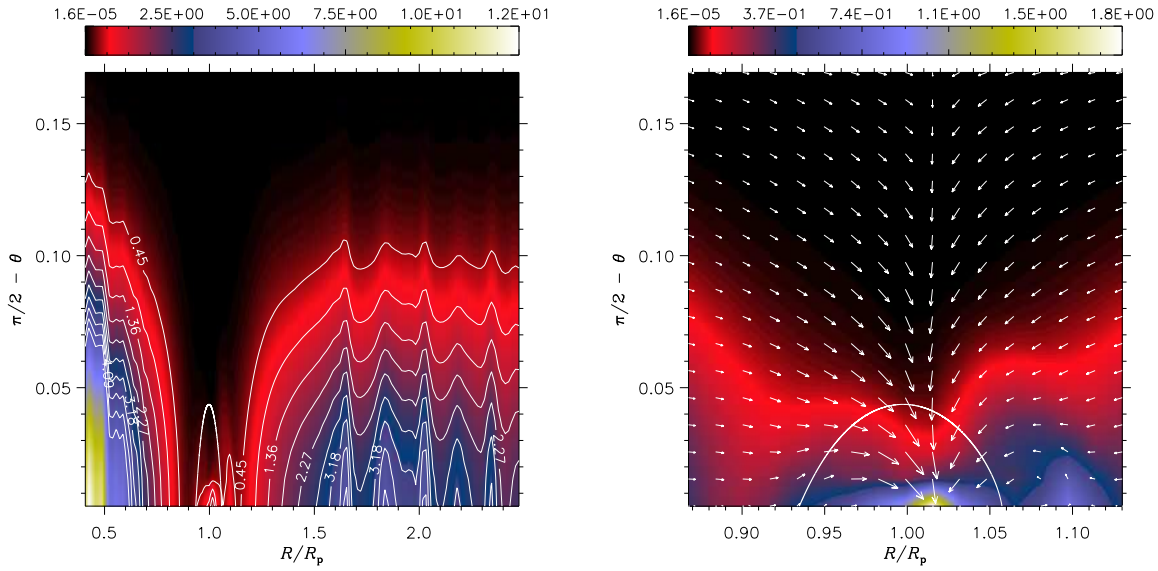

Fig. 5.— The density distribution and velocity field in the $r-\theta$ plane at $\varphi = \pi$ (where the planet is located) after 150 orbits. **Left:** Larger domain. **Right:** Enlargement of the region near the planet.

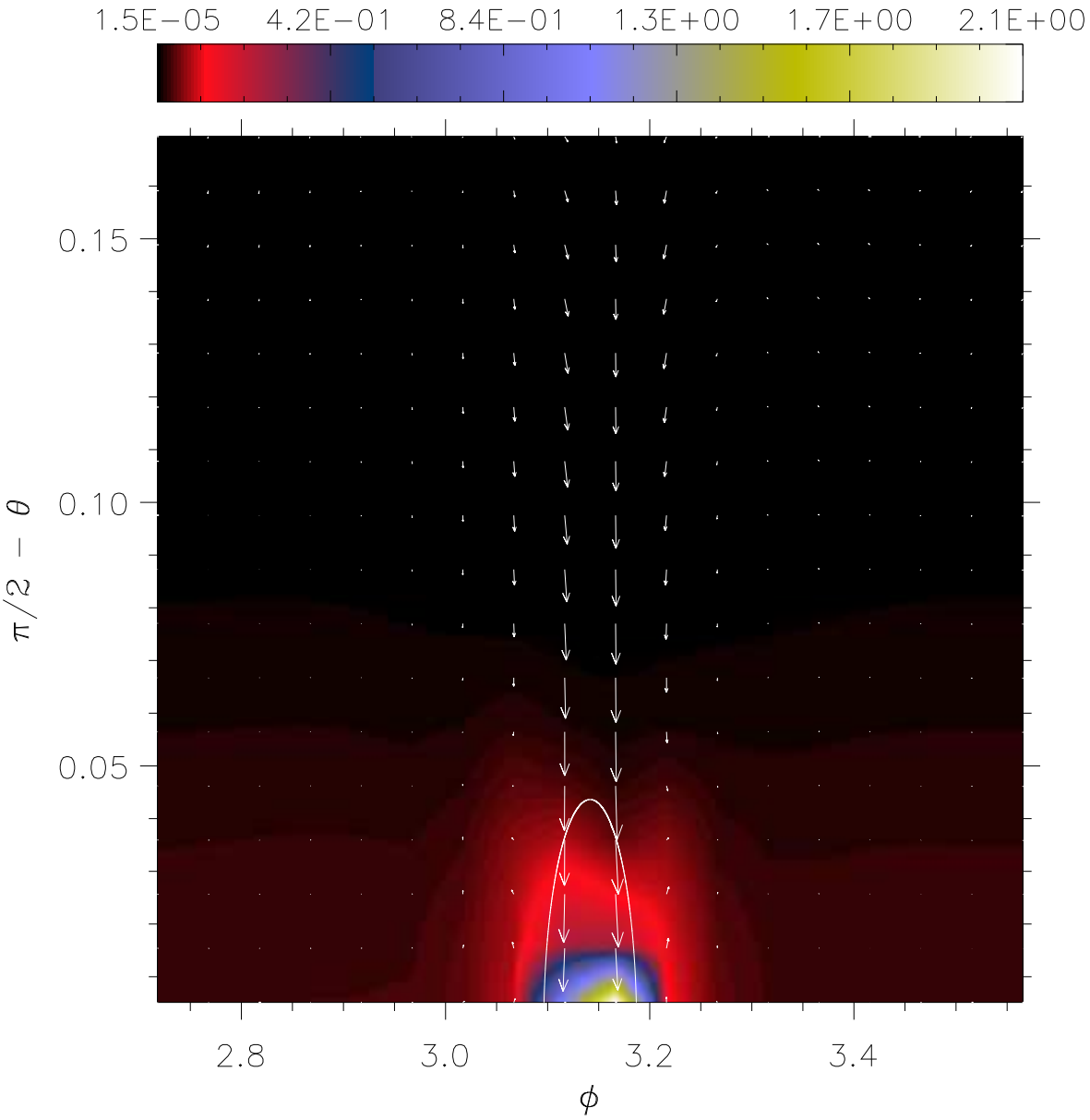

Fig. 6.— The density distribution and velocity field in the $\theta - \varphi$ plane at $R = 1$ (where the planet is located) after 150 orbits.

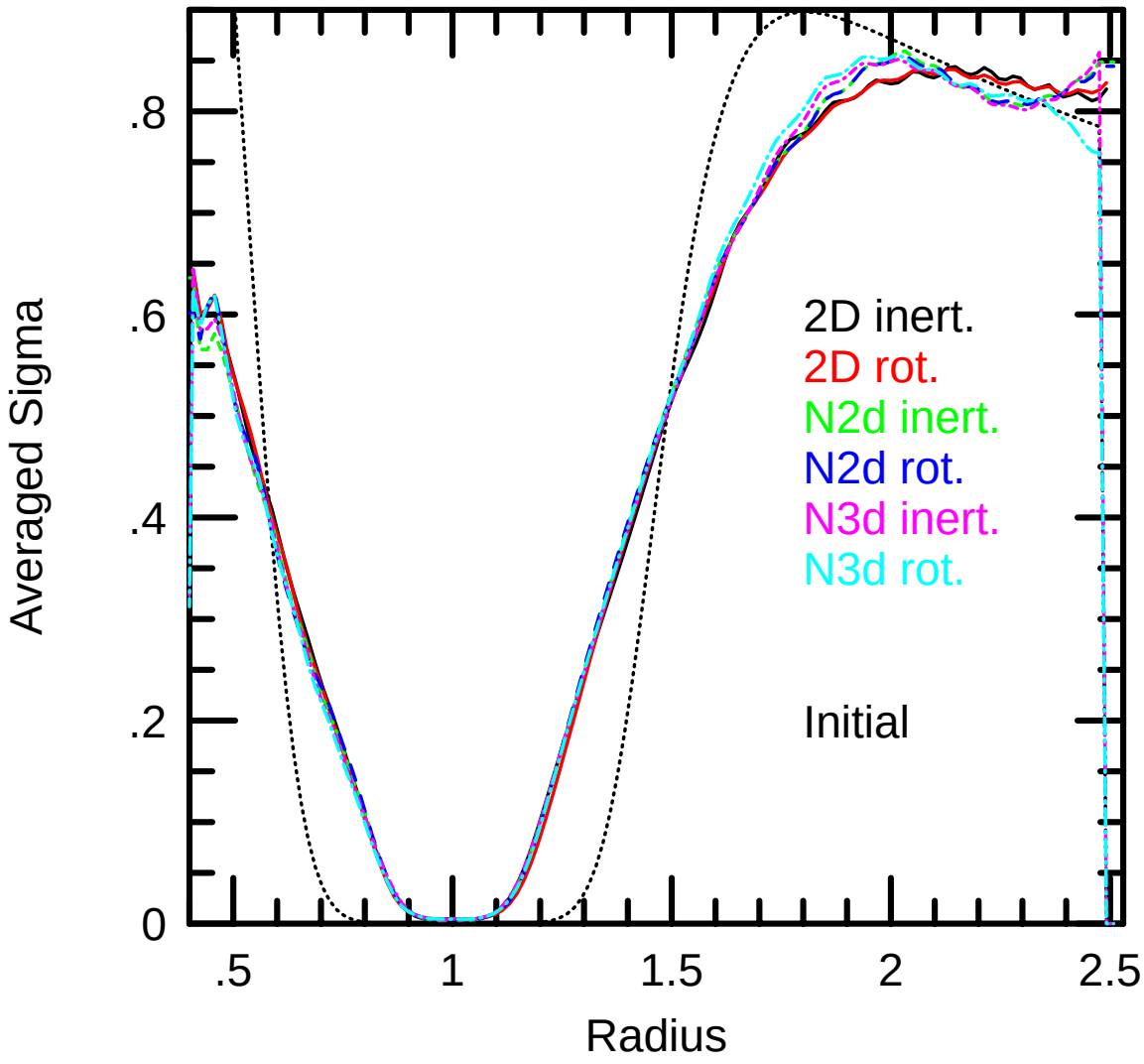

Fig. 7.— Azimuthally averaged surface density $\Sigma(r)$ after 150 orbital periods of the planet for three different models: 2D (code RH2D) solid lines, N2d (NIRVANA in 2D) dashed lines, and N3d (NIRVANA in 3D) dashed-dotted lines, each run in the inertial and cororating frame. The dark dotted line denotes the initial density profile.

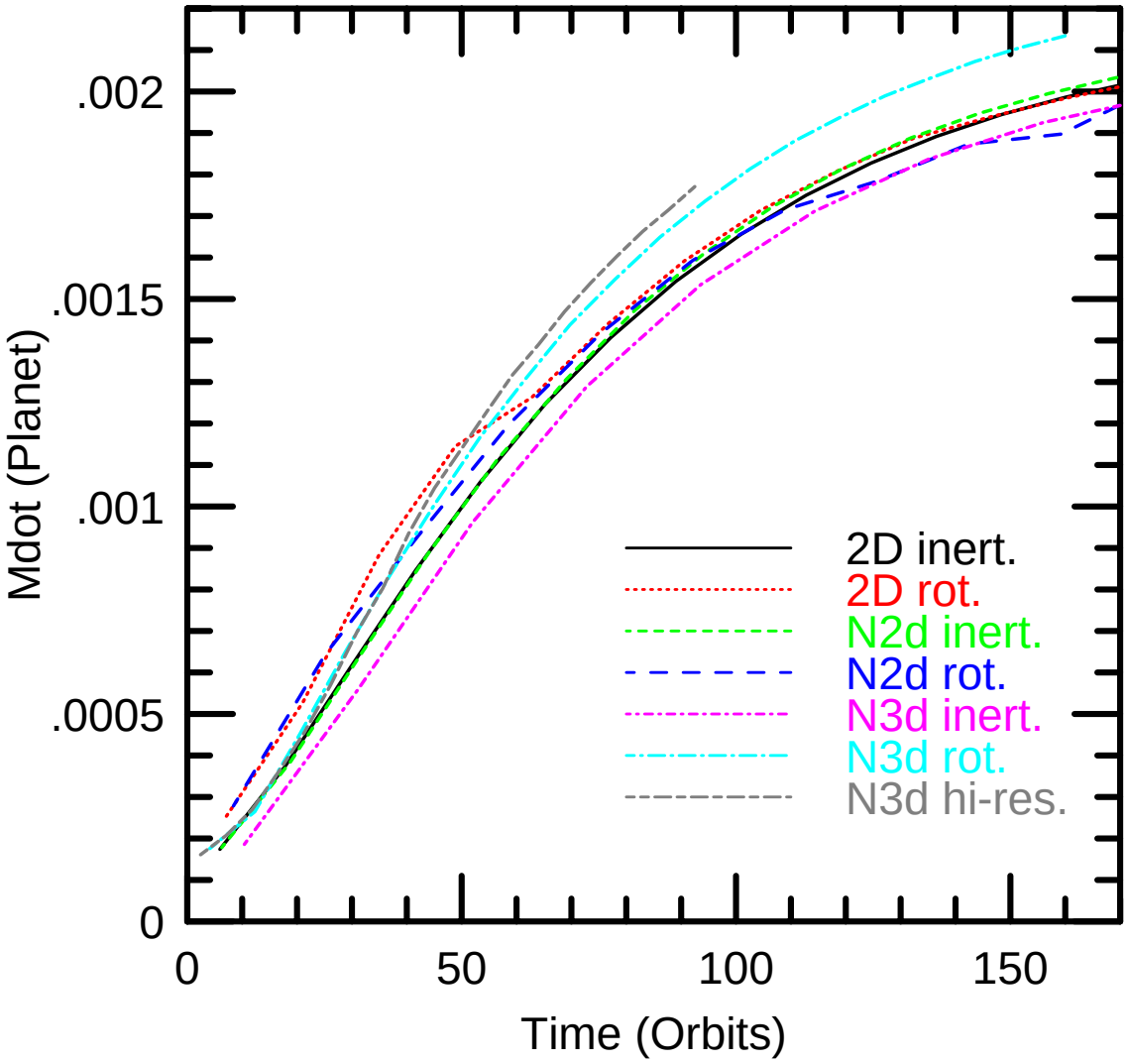

Fig. 8.— Mass accretion rate onto the planet in dimensionless units versus time for the models shown in Fig. 7. One high-resolution model (with 384 azimuthal gridcells) run in the rotating frame has been added.

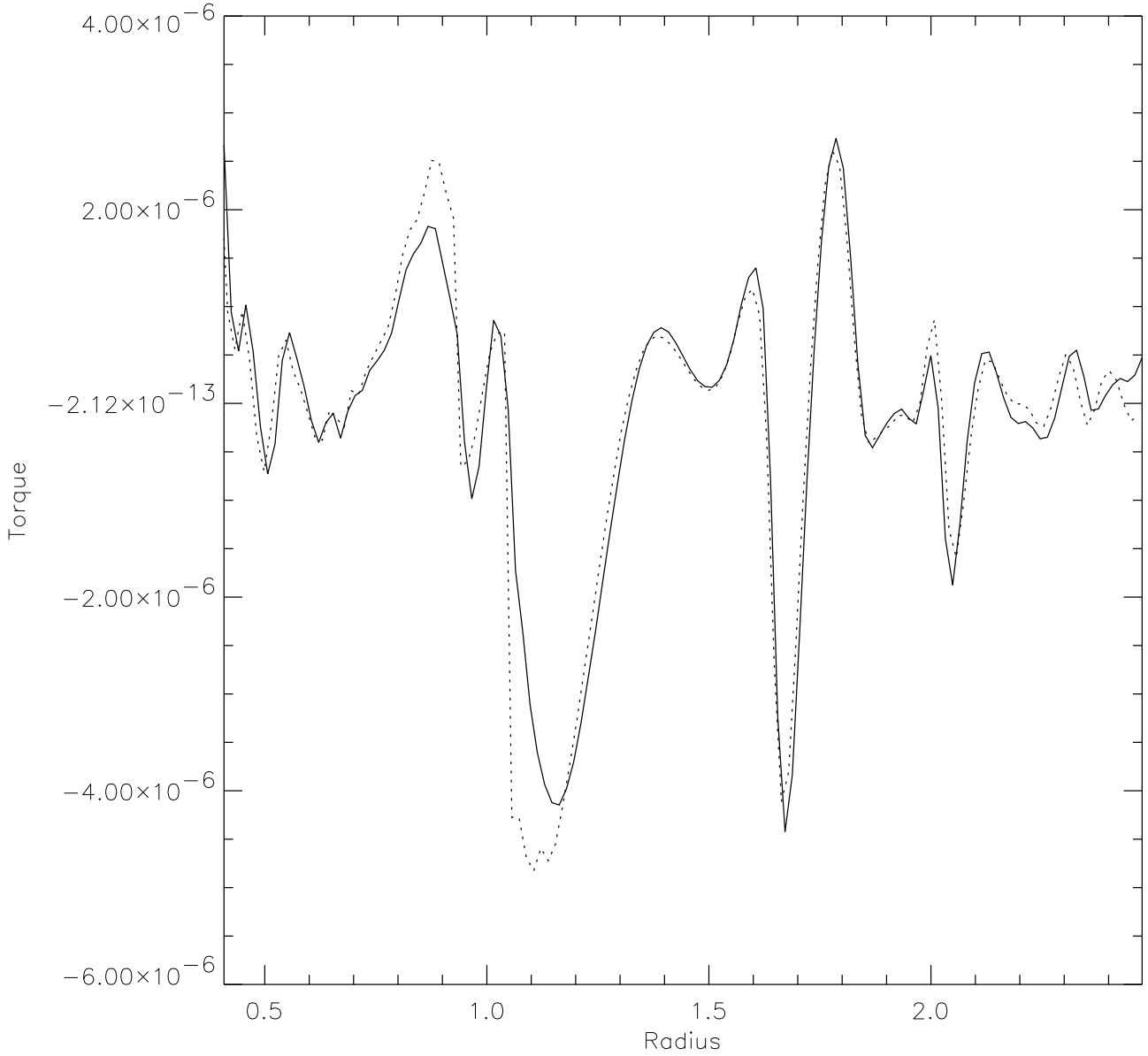

Fig. 9.— Radial distribution of the torque component T_z on the planet at time $t = 150$ orbits for the models N3D rot. (solid line) and N2D rot. (dotted line).

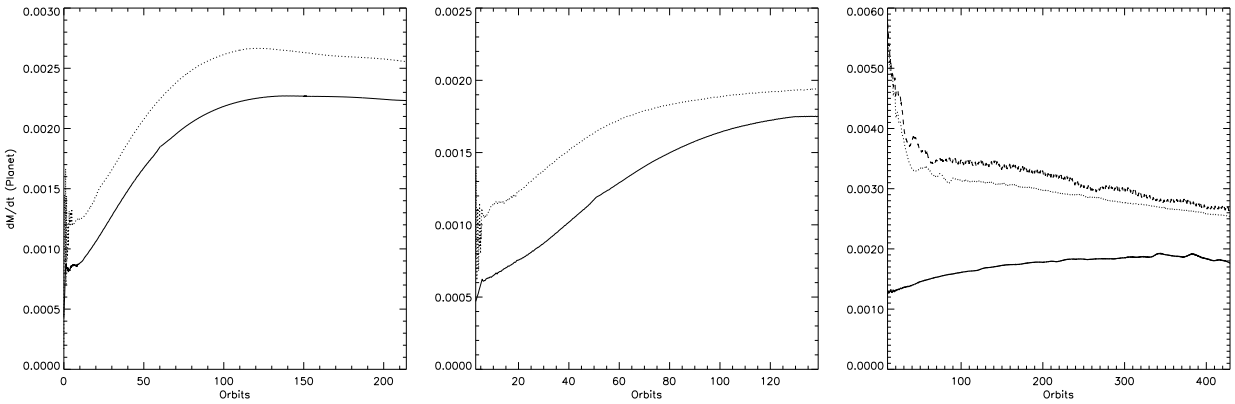

Fig. 10.— Mass accretion rates obtained from models listed in table 1. **Left panel**: Model B, solid line; Model A, dotted line. **Central panel**: Model C, solid line; Model D, dotted line. **Right panel**: Model P3, solid line; Model P2a, dotted line; Model P2b, dashed line.

4. Conclusion

We have performed 3D simulations of embedded Jupiter type planets in a protostellar disk of mass $M_d = 10^{-2} M_\odot$. We have shown that for a fully three-dimensional standard model, having the vertical disk thickness $H/r = 0.05$ and the constant (dimensionless) viscosity $\nu = 10^{-5}$, the obtained mass accretion rate $\dot{M}_p \approx 6 \times 10^{-5} M_{Jup}/yr$ and migration timescale of $\tau_{mig} \approx 10^5 yr$ are in very good agreement with corresponding 2D calculations. The value for the accretion rate $\dot{M}_p$ quoted in Kley (1999) is lower than the value obtained in this work because here we take into account the accretion from both sides of the disk while previously we considered only accretion from outside. Hence, we conclude that in this standard case the two-dimensional $(r - \varphi)$ calculations give an adequate representation of the evolution of planets in disks.

However, this agreement between 2D and 3D calculations can only be expected if the vertical extent of the Roche lobe of the planet is comparable to the disk thickness or larger, as for example for higher planetary masses. If the Roche lobe is much smaller than the disk thickness the gap will not be opened fully, and one may expect that some of the disk material will flow across the gap which is not fully cleared in these circumstances, and not end up onto the planet. This situation has been adressed with lower q and higher H/r models, and indeed we find a slightly reduced mass accretion onto the planet in these cases.

The present and previously published results concerning mass accretion and planet migration by ourselves and others, although in rough agreement with each other, may nevertheless suffer from insufficient resolution of the flow within and around the Roche-lobe of the planet. Once within the Roche lobe the gas will form a miniturized accretion disk around the planet. The question on how fast the accretion flow will be depends on the local viscosity within this sub-disk. If the disk is able to transport all the incoming material rapidly enough, the mass removal scheme used here will be satisfactory.

To address these questions much higher numerical resolutions possibly by applying methods of grid refinement will have to be used. Very interesting first results have been presented by Ciecieląg, Plewa & Różyczka (2000) but this issue definitely requires more work in the future.

We would like to thank Udo Ziegler for making the FORTRAN Version of his code NIRVANA (http://www.aip.de/groups/cap/software/nirvana/nirvana.html) available to us. This work was supported by the German Science Foundation (DFG) under grant KL 650/1-1. Some of the numerical computations have been carried out at the Computer Center of the Max-Planck Society in Garching (RZG) on a NEC-SX5 supercomputer.

Table 1. Parameters of the 2D (A, D, P2a, P2b) and 3D (B, C, P3) models used to compare the planet mass accretion rate.

Model	M_p[a]	H/r[b]	R-Range[c]	θ-Range	ΔR	$\Delta\theta$[d]	$\Delta\varphi$[e]
B	0.50	0.05	$[0.4, 2.5]$	$[80°, 90°]$	0.01640	0.01027	0.01653
A	0.50	0.05	$[0.4, 2.5]$		0.01640		0.01653
C	1.00	0.10	$[0.4, 2.5]$	$[70°, 90°]$	0.01640	0.00997	0.01653
D	1.00	0.10	$[0.4, 2.5]$		0.01640		0.01653
P3	1.00	0.15	$[0.4, 6.5]$	$[60°, 90°]$	0.04766	0.01939	0.04987
P2a	1.00	0.15	$[0.4, 6.5]$		0.04766		0.04987
P2b	1.00	0.15	$[0.4, 6.5]$		0.04766		0.01653

[a]The planet mass is normalized to the mass of Jupiter.

[b]r represents the distance from the rotational axis.

[c]The radial extent is given in units of the orbit semi-major axis a.

[d]The resolution is expressed in radians.

[e]$\varphi \in [0, 2\,\pi]$.

A. Numerical issues

The calculation are performed using the three-dimensional nested grid MHD-code NIRVANA (Ziegler & Yorke 1997; Ziegler 1998) in a FORTRAN Version. For the purpose of the present computations the magnetic part of the code has been omitted and the nested grid option has not been used. The finite difference code uses a conservative Eulerian formulation where the transport terms are based on the monotonic advection formulation originally developed by van Leer (1977). The viscosity part is treated explicitly and includes all tensor components. It has been used successfully in two-dimensional simulations of embedded Jupiter type planets where the focus was on migration and mass growth of the planet (Nelson et al. 2000). For some two-dimensional comparison computations we use the code RH2D as described in (Kley 1999).

We use dimensionless units where the radial distance of the planet to the star is normalized to one, i.e. $r_0 = 5.2$ AU, the unit of time is the inverse orbital frequency of the planet $t_0 = 1/\Omega_p$. The evolutionary times as quoted in the results section are typically given in units of the orbital period $P = 2\pi/\Omega_p$ of the planet. The density ρ_0 is normalized such that the total mass of the disk is $3.5 \times 10^{-3} M_\odot$.

The computational domain consists of a spherical polar section of the disk, extending radially from $R_{\rm min} = 0.4$ to $R_{\rm max} = 2.5$, meridionally from $\theta_{\rm min} = 80°$ to $\theta_{\rm max} = 90°$, and azimuthally from 0 to $2\,\pi$. Vertically, the computational domain has an extension of $10°$ measured from the equatorial plane, which is sufficient to include the whole disk. For the standard case the domain is covered by $(N_R, N_\theta, N_\varphi) = (128, 20, 128)$ grid cells, which are distributed equidistantly in R, θ and φ. For the higher resolution cases the number of azimuthal gridcells is increased to 384.

We have assumed reflection symmetry with respect to the equatorial plane, and simulate only the upper half of the disk. Azimuthally we use periodic boundary conditions, and in the radial direction we chose closed inner and outer boundaries.

The accretion of mass onto the planet is modelled by taking out some fraction (here 5×10^{-2}) of the mass from the inner half of the planet's Roche-lobe at each time step. This accreted material is monitored but it is not added to the dynamical mass of the planet.

REFERENCES

Beckwith S.V.W., Henning Th. & Nakagawa Y., 2000, in Protostars and Planets IV, ed. V. Mannings, A.P. Boss & S.S. Russell, (Tucson: Univ. Arizona Press), p533

Boss, A. P., 1998, EM&P, 81, 19

Bryden G., Chen X., Lin D.N.C, Nelson R.P. & Papaloizou J.C.B., 1999, ApJ, 514, 344

Butler R.P., Marcy G.W., Fischer D.A., Brown T.W., Contos A.R., Korzennik S.G., Nisenson P. & Noyes R.W., 1999, ApJ, 526, 916

Ciecieląg P., Plewa T. & Różyczka, M., 2000, in Disks, Planetesimals and Planets, ed F. Garzon, C. Eiroa, D. de Winter & T.J. Mahoney, to be published, astro-ph/0002029

Frank, J., King, A. & Raine, D., 1992, *Accretion Power in Astrophysics*, 2nd Edition, Cambridge Univ. Press.

Goldreich P. & Tremaine S., 1980, ApJ, 241, 425.

Klahr H.H., Henning Th. & Kley W. 1999, ApJ, 514, 325

Kley W. 1989, A&A, 208, 98

Kley W., 1998, A&A, 338, L37.

Kley W., 1999, MNRAS, 303, 696

Kley W., 2000, MNRAS, 313, L47

Lubow S.H., Seibert M. & Artymowicz P., 1999, ApJ, 526, 1001

Marcy G.W., Cochran W.D. & Mayor M., 2000, in Protostars and Planets IV, ed. V. Mannings, A.P. Boss & S.S. Russell, (Tucson: Univ. Arizona Press), p1285

Mayor M., Queloz D., Nature, 1995, 378, 355

Miyoshi K., Takeuchi T., Tanaka H., Ida S., 1999, ApJ, 516, 451

Nelson, A.F. & Benz W., 1999, in Proc. of Star Formation 1999, ed. T. Nakamoto, The Nobeyan Radiao Observatory, Nagoya, Japan, p251

Nelson, R., Papaloizou, J.C.B., Masset, F., Kley, W., 1999, MNRAS, in press, see astro-ph/9909486

Tassoul, J.-L., 1978, Theory of Rotating Stars, Princeton University Press

van Leer B., 1977, JCP, 89, 29

Ziegler U. & Yorke H.W., 1997, Comp. Phys. Comm., 101, 54

Ziegler U., 1998, Comp. Phys. Comm., 109, 111

This preprint was prepared with the AAS LaTeX macros v5.0.